Unstable manifolds of relative periodic orbits in the symmetry-reduced state space of the Kuramoto-Sivashinsky system

Nazmi Burak Budanur
Predrag Cvitanović

Abstract Systems such as fluid flows in channels and pipes or the complex Ginzburg-Landau system, defined over periodic domains, exhibit both continuous symmetries, translational and rotational, as well as discrete symmetries under spatial reflections or complex conjugation. The simplest, and very common symmetry of this type is the equivariance of the defining equations under the orthogonal group O(2). We formulate a novel symmetry reduction scheme for such systems by combining the method of slices with invariant polynomial methods, and show how it works by applying it to the Kuramoto-Sivashinsky system in one spatial dimension. As an example, we track a relative periodic orbit through a sequence of bifurcations to the onset of chaos. Within the symmetry-reduced state space we are able to compute and visualize the unstable manifolds of relative periodic orbits, their torus bifurcations, a transition to chaos via torus breakdown, and heteroclinic connections between various relative periodic orbits. It would be very hard to carry through such analysis in the full state space, without a symmetry reduction such as the one we present here.

Keywords Kuramoto-Sivashinsky equation · equivariant systems · relative periodic orbits · unstable manifolds · chaos · symmetries

PACS 02.20.-a · 05.45.-a · 05.45.Jn · 47.27.ed

Nazmi Burak Budanur
Institute of Science and Technology (IST), 3400 Klosterneuburg, Austria. E-mail: burak.budanur@ist.ac.at

Predrag Cvitanović
Center for Nonlinear Science, School of Physics, Georgia Institute of Technology, Atlanta, GA 30332-0430, USA.

1 Introduction

> "...of course, the motion of the system tends to move away from repellers. Nonetheless a repeller might be important because, for example, it might describe a separatrix that serves to divide two different attractors or two different types of motion." *Kadanoff and Tang [36]*.

The 1984 Kadanoff and Tang investigation of strange repellers was prescient in two ways. First, at the time it was not obvious why anyone would care about "repellers," as their dynamics would be transient. Today, much of the research in turbulence focuses on repellers. In particular, significant effort is invested in understanding the state space regions of shear-driven fluid flows that separate laminar and turbulent regimes [5, 21, 56, 60, 63], and these "separatrices" indeed often appear to be strange repellers. Kadanoff and Tang's study was quantitative, and modest by today's standards: they computed escape rates for a family of 3-dimensional mappings in terms of their unstable periodic orbits ('repulsive cycles'), while today corresponding computations are carried out for very high-dimensional ($\sim$100,000 computational degrees of freedom), numerically accurate discretizetions of Navier-Stokes flows [26, 27, 65]. In light of the heuristic nature of their investigation, their second insight was remarkable: they were the first to posit the *exact* weight for the contribution of an unstable periodic orbit p to an average computed over a strange repeller (or attractor):

$$1/|\det\left(\mathbf{1} - J_p(x)\right)|$$

(here $J_p(x)$ is the Jacobian matrix of linearized flow, computed along the orbit of a periodic point x). While, at the time, they were aware only of Bowen's (1975) work [7], today this formula is a cornerstone of the modern periodic orbit theory of chaos in deterministic flows [19], based on zeta functions of Smale (1967) [61], Gutzwiller (1969) [30], Ruelle (1976) [53, 54] and their cycle expansions (1987) [3, 4, 16, 43]. Much has happened since – in particular, the formulas of periodic orbit theory for 3-dimensional dynamics that they had formulated in 1983 are today at the core of the challenge very dear to Kadanoff, a dynamical theory of turbulence [14, 27]. For that to work, many extra moving parts come into play. We have learned that the convergence of cycle expansions relies heavily on the flow topology and the associated symbolic dynamics, and that understanding the geometry of flows in the state space is the first step towards extending periodic orbit theory to systems of high or infinite dimensions, such as fluid flows. It turns out that taking care of the symmetries of a nonlinear fluid flow is also a difficult problem. While one can visualize dynamics in 2 or 3 dimensions, the state space of these flows is high-dimensional, and symmetries -both continuous and discrete- complicate the flow geometry as each solution comes along with all of its symmetry copies. In this contribution to Leo Kadanoff memorial volume, we develop new tools for investigating geometries of flows with symmetries, and illustrate their utility by applying them to a spatiotemporally chaotic Kuramoto-Sivashinsky system.

Originally derived as a simplification of the complex Ginzburg-Landau equation [40] and in study of flame fronts [59], the Kuramoto-Sivashinsky is perhaps the simplest spatially extended dynamical system that exhibits spatiotemporal chaos. Similar in form to the Navier-Stokes equations, but much easier computationally, the Kuramoto-Sivashinsky partial differential equation (PDE) is a convenient

sandbox for developing intuition about turbulence [33]. As for the Navier-Stokes, a state of the Kuramoto-Sivashinsky system is usually visualized by its shape over configuration space (such as states shown in fig. 1). However, the function space of allowable PDE fields is an infinite-dimensional state space, with the instantaneous state of the field a point in this space. In spite of the state space being high (and even infinite) dimension, evolution of the flow can be visualized, as generic trajectories are 1-dimensional curves, and numerically exact solutions such as equilibria and periodic orbits are points or closed loops, in any state space projection. There are many choices of a "state space." Usually one starts out with the most immediate one: computational elements used in a finite-dimensional discretization of the PDE studied. As the Kuramoto-Sivashinsky system in one space dimension, with periodic boundary condition, is equivariant under continuous translations and a reflection, for the case at hand the natural choice is a Fourier basis, truncated to a desired numerical accuracy. This is still a high-dimensional space: in numerical work performed here, 30-dimensional. For effective visualizations, one thus needs to carefully pick dynamically intrinsic coordinate frames, and projections on them [17, 27].

Such dynamical systems visualisations of turbulent flows, complementary to the traditional spatio-temporal visualizations, offer invaluable insights into the totality of possible motions of a turbulent fluid. However, symmetries, and especially continuous symmetries, such as equvariance of the defining equations under spatial translations, tend to obscure the state space geometry of the system by their preference for higher-dimensional invariant N-tori solutions, such as relative equilibria and relative periodic orbits.

In order to avoid dealing with such effects of continuous symmetry, a number of papers [14, 41, 50–52] study the Kuramoto-Sivashinsky equation within the flow-invariant subspace of solutions symmetric under reflection. However, such restrictions to flow-invariant subspaces miss the physics of the problem: any symmetry invariant subspace is of zero measure in the full state space, so a generic turbulent trajectory explores the state space *outside* of it. Lacking continuous-symmetry reduction schemes, earlier papers on the geometry of the Kuramoto-Sivashinsky flow in the full state space [1, 17, 29, 37] were restricted to the study of the smallest invariant structures: equilibria, their stable/unstable manifolds, their heteroclinic connections, and their bifurcations under variations of the domain size.

Stationary solutions are important for understanding the state space geometry of a chaotic attractor, as their stable manifolds typically set the boundaries of the strange set. The Lorenz attractor is the best known example [64] and Gibson *et al.* [27] visualizations for the plane Couette flow are so far the highest-dimensional setting, where this claim appears to hold. In this paper we turn our attention to (relative) periodic orbits, which –unlike unstable equilibria– are embedded within the strange set, and are expected to capture physical properties of an ergodic flow. Refs. [14, 41], restricted to the reflection-invariant subspace of the Kuramoto-Sivashinsky flow, have succeeded in constructing symbolic dynamics for several system sizes. In these examples, short periodic orbits have real Floquet multipliers, with very thin unstable manifolds, around which the longer periodic orbits are organized by means of nearly 1-dimensional Poincaré return maps.

In this paper we study the unstable manifolds of relative periodic orbits of Kuramoto-Sivashinsky system in full state space, with no symmetry restrictions. In contrast to the flow-invariant subspace considered in refs. [14, 41], the shortest rela-

tive periodic orbit of the full system that is stable for small system sizes ($L < 21.22$) has a complex leading Floquet multiplier. This renders the associated unstable manifold 2-dimensional. Elimination of the marginal directions, the space and time translation symmetries, by a 'slice' and a Poincaré section conditions, together with a novel reduction of the spatial reflection symmetry, enables us to study here this 2-dimensional unstable manifold. We compute and visualize the unstable manifold of the shortest periodic orbit as we increase the system size towards the system's transition to chaos.

Summary of our findings is as follows: At the system size $L \approx 21.22$, the shortest periodic orbit undergoes a torus bifurcation [34] (also sometimes referred to as the Neimark-Sacker bifurcation [46, 55], if the flow is studied in a Poincaré section), which gives birth to a stable 2-torus. As the system size is increased, this torus first goes unstable, and is eventually destroyed by the bifurcation into stable and unstable pair of period-3 orbits, to which the unstable manifold of the parent orbit is heteroclinically connected. As the system size is increased further, the stable period-3 orbit goes unstable, then disappears, and the dynamics becomes chaotic. Upon a further increase of the system size, the unstable period 3 orbit undergoes a symmetry-breaking bifurcation, which introduces richer dynamics as the associated unstable manifold has connections to both drifting (relative) and non-drifting periodic orbits.

We begin by a short review of the Kuramoto-Sivashinsky system in the next section, and review continuous symmetry reduction by first Fourier mode slice method in section 3.1. The main innovation introduced in this paper is the invariant polynomial discrete symmetry reduction method described in section 3.2. The new symmetry reduction method is applied to and tested on the Kuramoto-Sivashinsky system in section 4, where the method makes it possible to track the evolution of the periodic orbits unstable manifolds through the system's transition to chaos. We discuss the implications of our results and possible future directions in section 5.

2 Kuramoto-Sivashinsky system and its symmetries

We study the Kuramoto-Sivashinsky equation in one space dimension

$$u_\tau = -u\,u_x - u_{xx} - u_{xxxx}\,, \tag{1}$$

with periodic boundary condition $u(x,\tau) = u(x+L,\tau)$. The real field $u(x,\tau)$ is the "flame front" velocity [59]. The domain size L is the bifurcation parameter for the system, which exhibits spatiotemporal chaos for sufficiently large L: see fig. 1 (e) for a typical spatiotemporally chaotic trajectory of the system at $L = 22$.

We discretize the Kuramoto-Sivashinsky system by Fourier expanding the field $u(x,\tau) = \sum_k \tilde{u}_k(\tau)e^{iq_k x}$, and expressing (1) in terms of Fourier modes as an infinite set of ordinary differential equations (ODEs)

$$\dot{\tilde{u}}_k = (q_k^2 - q_k^4)\,\tilde{u}_k - i\frac{q_k}{2}\sum_{m=-\infty}^{+\infty}\tilde{u}_m\tilde{u}_{k-m}\,, \quad q_k = \frac{2\pi k}{L}\,. \tag{2}$$

Kuramoto-Sivashinsky equation is *Galilean invariant*: if $u(x,\tau)$ is a solution, then $v + u(x - v\tau, \tau)$, with v an arbitrary constant velocity, is also a solution.
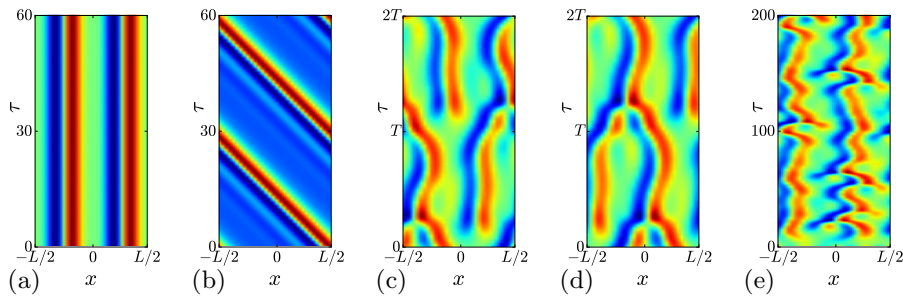
Fig. 1 Examples of invariant solutions of the Kuramoto-Sivashinsky system and the chaotic flow visualized as the color coded amplitude of the scalar field $u(x,\tau)$: (a) Equilibrium E_1, (b) Relative equilibrium TW_1, (c) Pre-periodic orbit with period $T = 32.4$, (d) Relative periodic orbit with period $T = 33.5$. (e) Chaotic flow. Horizontal and vertical axes correspond to space and time respectively. System size $L = 22$. The invariant solutions and their labels are taken from ref. [17].

In the Fourier representation (2), the Galilean invariance implies that the zeroth Fourier mode $\tilde{u}_0$ is decoupled from the rest and time-invariant. Hence, we exclude $\tilde{u}_0$ from the state space and represent a Kuramoto-Sivashinsky state $u = u(x,\tau)$ by the Fourier series truncated at $k = N$, i.e., a $2N$-dimensional real valued state space vector

$$a = (b_1, c_1, b_2, c_2, \ldots, b_N, c_N) \,, \tag{3}$$

where $b_k = \mathrm{Re}\,[\tilde{u}_k]$, $c_k = \mathrm{Im}\,[\tilde{u}_k]$. One can rewrite (2) in terms of this real valued state space vector, and express the truncated set of equations compactly as

$$\dot{a} = v(a) \,. \tag{4}$$

In our numerical work we use a pseudo-spectral formulation of (4), described here in appendix A, and in detail in the appendix of ref. [17].

Spatial translations $u(x,\tau) \to u(x + \delta x, \tau)$ on a periodic domain correspond to SO(2) rotations $a \to D(g(\theta))\,a$ in the Kuramoto-Sivashinsky state space, with the matrix representation

$$D(g(\theta)) = \mathrm{diag}\,[\,R(\theta),\, R(2\theta),\, \ldots,\, R(N\theta)\,] \,, \tag{5}$$

where $\theta = 2\pi\delta x/L$ and

$$R(k\theta) = \begin{pmatrix} \cos k\theta & -\sin k\theta \\ \sin k\theta & \cos k\theta \end{pmatrix}$$

are $[2 \times 2]$ rotation matrices. Kuramoto-Sivashinsky dynamics commutes with the action of (5), as can be verified by checking that (4) satisfies the equivariance relation

$$v(a) = D^{-1}(g(\theta))v(D(g(\theta))a) \,. \tag{6}$$

By the translation symmetry of the Kuramoto-Sivashinsky system, each solution of PDE (1) has infinitely many dynamically equivalent copies that can be obtained by translations (5). Systems with continuous symmetries thus tend to have higher-dimensional invariant solutions: relative equilibria (traveling waves) and relative

periodic orbits. A *relative equilibrium* evolves only along the continuous symmetry direction

$$a_{tw}(\tau) = D(g(\tau \dot{\theta}_{tw})) \, a_{tw}(0) \, ,$$

where $\dot{\theta}_{tw}$ is a constant phase velocity, and the suffix tw indicates that the solution is a "traveling wave." A *relative periodic orbit* recurs exactly at a symmetry-shifted location after one period

$$a_{rp}(0) = D(g(-\theta_{rp})) \, a_{rp}(T_{rp}) \, . \tag{7}$$

Fig. 1 (b) and (d) show space-time visualizations of a Kuramoto-Sivashinsky relative equilibrium and a relative periodic orbit. The sole dynamics of a relative equilibrium is a constant drift along the continuous symmetry direction, while a relative periodic orbit shifts by amount θ_{rp} for each repeat of its period, and traces out a torus in the full state space.

The Kuramoto-Sivashinsky equation (1) has no preferred direction, and is thus also equivariant under the *reflection* symmetry $u(x, \tau) \to -u(-x, \tau)$: for each solution drifting left, there is a reflection-equivalent solution which drifts right. In terms of Fourier components, the reflection σ acts as complex conjugation followed by a negation, whose action on vectors in state space (3) is represented by the diagonal matrix

$$D(\sigma) = \mathrm{diag} \, [\, -1, \, 1, \, -1, \, 1, \, \ldots, \, -1, \, 1 \,] \, , \tag{8}$$

which flips signs of the real components b_i. Due to this reflection symmetry, the Kuramoto-Sivashinsky system can also have strictly non-drifting equilibria and (pre-)periodic orbits. An *equilibrium* is a stationary solution $a_{eq}(\tau) = a_{eq}(0)$. A *periodic orbit* p is periodic with period T_p, $a_p(0) = a(T_p)$, and a *pre-periodic orbit* is a relative periodic orbit

$$a_{pp}(0) = D(\sigma) \, a_{pp}(T_{pp}) \tag{9}$$

which closes in the full state space after the second repeat, hence we refer to it here as 'pre-periodic'.

In fig. 1 (a) we show equilibrium E_1 of Kuramoto-Sivashinsky equation (so labelled in ref. [17]). If we were to take the mirror image of fig. 1 (a) with respect to $x = 0$ line, and then interchange red and blue colors, we would obtain the same solution; all equilibria belong to the flow-invariant subspace of solutions invariant under the reflection symmetry of the Kuramoto-Sivashinsky equation. Similar to equilibria, time-periodic solutions of the Kuramoto-Sivashinsky equation that are not repeats of pre-periodic ones (9) also belong to the reflection-invariant subspace. See [14, 41, 50–52] for examples of such solutions. Fig. 1 (b) shows a pre-periodic solution of the Kuramoto-Sivashinsky system: dynamics of the second period can be obtained from the first one by reflecting it. Both equilibria and pre-periodic orbits have infinitely many copies that can be obtained by continuous translations, symmetric across the shifted symmetry line, $g(\theta)\sigma g(-\theta)$. Note that reflection σ and translations $g(\theta)$ do not commute: $\sigma \, g(\theta) = -g(\theta) \, \sigma$, or, in terms of the generator of translations, the reflection reverses the direction of the translation, $\sigma \, T = -T \, \sigma$. Let $f^\tau(a)$ denote the finite-time flow induced by (4), and let a_{pp} belong to a pre-periodic orbit defined by (9). Then the shifted point $a'_{pp} = D(g(\theta)) \, a_{pp}$ satisfies

$$f^{T_p}(a'_{pp}) = D(g(\theta))D(\sigma)D(g(-\theta)) \, a'_{pp} \, .$$

In contrast, a relative periodic orbit (7) has a distinct reflected copy $a'_{rp} = D(\sigma)a_{rp}$ with the reverse phase shift:

$$a'_{rp}(0) = D(g(\theta_p))\, a'_{rp}(T_p)\,.$$

In order to carry out our analysis, we must first eliminate all these degeneracies. This we do by symmetry reduction, which we describe next.

3 Symmetry reduction

A group orbit of state a is the set of all state space points reached by applying all symmetry actions to a. *Symmetry reduction* is any coordinate transformation that maps each group orbit to a unique state space point $\tilde{a}$ in the symmetry-reduced state space. For the O(2) symmetry considered here, we achieve this in two steps: We first reduce continuous translation symmetry of the system by method of slices, and then reduce the remaining reflection symmetry by constructing an invariant polynomial basis.

To the best of our knowledge, Cartan[12] was first to use method of slices in purely differential geometry context and early appearances of slicing methods in dynamical systems literature are works of Field[24] and Krupa[39]. Our implementation of the method of slices for SO(2) symmetry reduction follows ref. [11]. For a more exhaustive review of the literature we refer the reader to ref. [19].

Invariant polynomial or 'integrity' bases[13, 25] are a standard tool[31, 47] for orbit space reduction. They work very well in low dimensions[10, 13, 28, 58], but in high dimensions integrity bases are high-order polynomials of the original state space coordinates, accompanied by large numbers of nonlinear syzygies that confine the symmetry-reduced dynamics to lower-dimensional manifolds. These make the geometry of the reduced state space complicated and hard to work with for applications we have in mind here, such as visualizations of unstable manifolds of invariant solutions. Even with the use of computer algebra[25], constructing an O(2)-invariant integrity basis becomes impractical for systems of dimension higher than ~ 12. In spatio-temporal and fluid dynamics applications the corresponding n (Fourier series truncation) is easily of order 10-100. The existing methods for construction of such integrity bases are neither feasible for higher-dimensional state spaces[57] (we need to reduce symmetry for 10^5-10^6-dimensional systems[27, 66]), nor helpful for reduced state space visualizations (m-th Fourier coefficient is usually replaced by a polynomial of order m).

Here we avoid constructing such high-order O(2) polynomial integrity bases by a hybrid approach. We reduce the continuous symmetry by the first Fourier mode slice in section 3.1, and *then* reduce the remaining reflection symmetry by a transformation to invariant polynomials in section 3.2. The resulting polynomials are only second order in the original state space coordinates, with no syzygies.

3.1 SO(2) symmetry reduction

Following ref. [11], we reduce the SO(2) symmetry of the Kuramoto-Sivashinsky equation by implementing the *first Fourier mode slice* method, i.e., by rotating the

Fourier modes as

$$\hat{a}(\tau) = D(g(\phi(\tau))^{-1})\, a(\tau)\,, \qquad (10)$$

where $\phi(\tau) = \arg(\tilde{u}_1(\tau))$ is the phase of the first Fourier mode. This transformation exists as long as the first mode in the Fourier expansion (10) does not vanish, $b_1^2 + c_1^2 > 0$, and its effect is to fix the phase of the first Fourier mode to zero for all times, as illustrated in fig. 2. The SO(2)-reduced state space is one dimension lower than the full state space, with coordinates

$$\hat{a} = (\hat{b}_1, 0, \hat{b}_2, \hat{c}_2, \dots \hat{b}_N, \hat{c}_N)\,. \qquad (11)$$

The dynamics within the first Fourier mode slice is given by

$$\dot{\hat{a}} = \hat{v}(\hat{a}) = v(\hat{a}) - \frac{\dot{c}_1}{\hat{b}_1}\, T\hat{a}\,, \qquad (12)$$

where T is the generator of infinitesimal SO(2) transformations, $D(g(\theta)) = \exp T\theta$, and $\dot{c}_1$ is full state space orbit's out-of-slice velocity, the second element of the velocity field (4). Symmetry-reduced state space velocity (12) diverges when the amplitude $\hat{b}_1$ of the first Fourier mode tends to 0. If $\hat{b}_1$ were 0, then the transformation (10) would no longer be uniquely defined. However, our experience had been such that this does not happen for generic trajectories of a chaotic system; and the singularity in the vicinity of $\hat{b}_1 = 0$ can be regularized by a time-rescaling transformation [11]. For further details we refer the reader to refs. [10, 11, 19].

Fig. 2 A sketch of the full state space trajectory $a(\tau)$ (blue and red) projected onto the first Fourier mode subspace (b_1, c_1), with rotation phases $\phi(\tau_1), \phi(\tau_2)$ at times τ_1 and τ_2, see (10). In this 2-dimensional projection we are looking at the symmetry-reduced state space "from the top"; the symmetry-reduced orbit is confined to the horizontal half-axis ($\hat{b}_1 > 0$, $\hat{c}_1 = 0$), and the remaining $2N-2$ coordinates are all projected onto the origin.
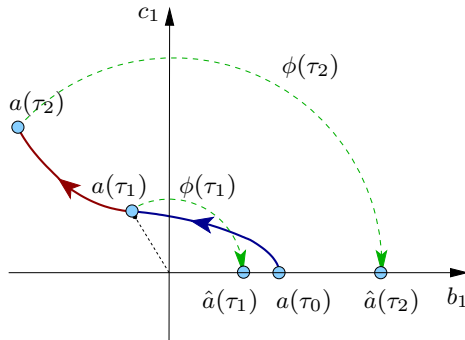
3.2 O(2) symmetry reduction

Our next challenge is to devise a transformation from (11) to discrete-symmetry-reduced coordinates, where the equivariance under reflection is also reduced. Consider the action of reflection on the SO(2)-reduced state space. In general, a slice is an arbitrarily oriented hyperplane, and action of the reflection σ can be rather complicated: it maps points within the slice hyperplane into points outside of it, which then have to be rotated into the slice. However, the action of σ on the first Fourier mode slice is particularly simple. Reflection operation $D(\sigma)$ of (8) flips the sign of the first SO(2)-reduced state space coordinate in (11), i.e., makes the

phase of the first Fourier mode π. Rotating back into the slice by (10), we find that within the first Fourier mode slice, the reflection acts by alternating the signs of even (real part) and odd (imaginary part) Fourier modes:

$$
\begin{aligned}
\hat{D}(\sigma) &= D(g(-\pi))D(\sigma) \\
&= \mathrm{diag}\,[\,1,\,-1,\,-1,\,1,\,1,\,-1,\,-1,\,1,\,1,\,\ldots]\,.
\end{aligned} \tag{13}
$$

The action on the slice coordinates (where we for brevity omit all terms whose signs do not change under reflection) is thus

$$
\begin{aligned}
\hat{D}(\sigma)\ &(\hat{b}_2, \hat{c}_3, \hat{b}_4, \hat{c}_5, \hat{b}_6, \hat{c}_7, \ldots) \\
&= (-\hat{b}_2, -\hat{c}_3, -\hat{b}_4, -\hat{c}_5, -\hat{b}_6, -\hat{c}_7, \ldots)\,.
\end{aligned} \tag{14}
$$

Our task is now to construct a transformation to a set of coordinates invariant under (14). One could declare a half of the symmetry-reduced state space to be a 'fundamental domain' [19], with segments of orbits that exit it brought back by reflection, but this makes orbits appear discontinuous and the dynamics hard to visualize. Instead, here we shall reduce the reflection symmetry by constructing polynomial invariants of coordinates (14). Squaring (or taking absolute value of) each sign-flipping coordinate in (14) is not an option, since such coordinates would be invariant under every individual sign change of these coordinates, and that is not a symmetry of the system. We are allowed to impose *only one* condition to reduce the 2-element group orbit of the discrete reflection subgroup of O(2). How that can be achieved is suggested by Miranda and Stone [28, 45] reduction of C_2 symmetry $(x, y, z) \to (-x, -y, z)$ of the Lorenz flow. They construct the symmetry-reduced "proto-Lorenz system" by transforming coordinates to the polynomial basis

$$
u = x^2 - y^2\,, \quad v = 2xy\,, \quad z = z\,. \tag{15}
$$

The x coordinate can be recovered from u and v of (15) up to a choice of sign, i.e., up to the original reflection symmetry. We extend this approach in order to achieve a 2–to–1 symmetry reduction for Kuramoto-Sivashinsky system: we construct the first coordinate from squares, but then 'twine' the successive sign-flipping terms $(\hat{b}_2, \hat{c}_3, \hat{b}_4, \hat{c}_5, \hat{b}_6, \hat{c}_7, \ldots)$ into second-order invariant polynomials basis set

$$
\begin{aligned}
(p_2, &\, p_3, p_4, p_5, p_6, \ldots) \\
&= (\hat{b}_2^2 - \hat{c}_3^2,\ \hat{b}_2\hat{c}_3,\ \hat{b}_4\hat{c}_3,\ \hat{b}_4\hat{c}_5,\ \hat{b}_5\hat{c}_6,\ \ldots)\,.
\end{aligned} \tag{16}
$$

The original coordinates can be recovered recursively by the 1–to–2 inverse transformation

$$
\begin{aligned}
b_2 &= \pm\sqrt{\frac{p_2 + \sqrt{p_2^2 + 4p_3^2}}{2}} \\
c_3 &= p_3/b_2\,, \quad b_4 = p_4/c_3\,, \quad c_5 = p_5/b_4\,, \quad \cdots\,.
\end{aligned}
$$

To summarize: we first reduce the group orbits generated by the continuous SO(2) symmetry subgroup by implementing the first Fourier mode slice (10), and then reduce the group orbits of the discrete 2-element reflection subgroup by replacing the sign-changing coordinates (14) with the invariant polynomials (16). The final O(2) symmetry-reduced coordinates are

$$
\tilde{a} = (\hat{b}_1, 0, \hat{b}_2^2 - \hat{c}_3^2, \hat{c}_2, \hat{b}_3, \hat{b}_2\hat{c}_3, \hat{b}_4\hat{c}_3, \hat{c}_4, \hat{b}_5, \ldots)\,. \tag{17}
$$

L	p_0		p_1		p_2	
	μ	θ	μ	θ	μ	θ
21.25	6.443×10^{-4}	± 2.177	–		–	
21.30	1.839×10^{-3}	± 2.158	–		–	
21.36	1.839×10^{-3}	± 2.158	5.854×10^{-3}	0	-1.623×10^{-3}	± 0.3098
			-8.357×10^{-3}	0		
21.48	7.638×10^{-3}	± 2.097	1.307×10^{-2}	0	–	
			-1.234×10^{-2}	0		
21.70	1.739×10^{-2}	± 2.044	2.521×10^{-2}	0	–	
			4.157×10^{-3}	π		

Table 1 The two leading non-marginal Floquet multipliers $\Lambda = \exp(T\mu + i\theta)$ of periodic orbits p_0, p_1, p_2 for system sizes L studied here. Dash – indicates that the orbit is not found for the corresponding system size.

Here pairs of orbits related by reflection σ are mapped into a single orbit, and $\hat{c}_1$ is identically set to 0 by continuous symmetry reduction, thus the symmetry-reduced state space has one dimension less than the full state space.

The symmetry-reduced state space (17) retains all physical information of the Kuramoto-Sivashinsky system: relative equilibria and relative periodic orbits of the original system become equilibria and periodic orbits in the symmetry-reduced state space (17), and pre-periodic orbits close after one period. For this reason, in what follows we shall refer to both relative periodic orbits and pre-periodic orbits as 'periodic orbits', unless we comment on their specific symmetry properties.

4 Unstable manifolds of periodic orbits

In order to demonstrate the utility, and indeed, the necessity of the O(2) symmetry reduction, we now investigate the transition to chaos in the neighborhood of a short Kuramoto-Sivashinsky pre-periodic orbit, focusing on the parameter range $L \in [21.0, 21.7]$. Our method yields a symmetry-reduced velocity field $\tilde{v}(\tilde{a}) = \dot{\tilde{a}}$ and a finite-time flow $\tilde{f}^\tau(\tilde{a}(0)) = \tilde{a}(\tau)$ in the symmetry-reduced state space (17). Although we can obtain $\tilde{v}(\tilde{a})$ by chain rule, we find its numerical integration unstable, hence in practice we obtain $\tilde{v}(\tilde{a})$ and $\tilde{f}^\tau(\tilde{a})$ from the first Fourier mode slice by applying the appropriate Jacobian matrices, as described in appendix A.

At $L = 21.0$, the Kuramoto-Sivashinsky system has a stable periodic orbit p_0, which satisfies $\tilde{a}_{p_0} = \tilde{f}^{T_{p_0}}(\tilde{a}_{p_0})$ for any point $\tilde{a}_{p_0}$ on the periodic orbit p_0. Linear stability of a periodic orbit is described by the Floquet multipliers Λ_i and Floquet vectors $\tilde{V}_i$,1 which are the eigenvalues and eigenvectors of the Jacobian matrix $\tilde{J}_p$ of the finite-time flow $\tilde{f}^{T_p}(\tilde{a}_p)$

$$\tilde{J}_p \tilde{V}_i = \Lambda_i \tilde{V}_i \,.$$

Each periodic orbit has at least one marginal Floquet multiplier $\Lambda_v = 1$, corresponding to the velocity field direction. When $L < 21.22$, all other Floquet multipliers of p_0 have absolute values less than 1. At $L \approx 21.22$, leading complex pair of Floquet multipliers $\Lambda_{1,2}$ crosses the unit circle, and the corresponding eigenplane

spanned by the real and imaginary parts of $\tilde{V}_1$ develops 'spiral out' dynamics that connects to a 2-torus.
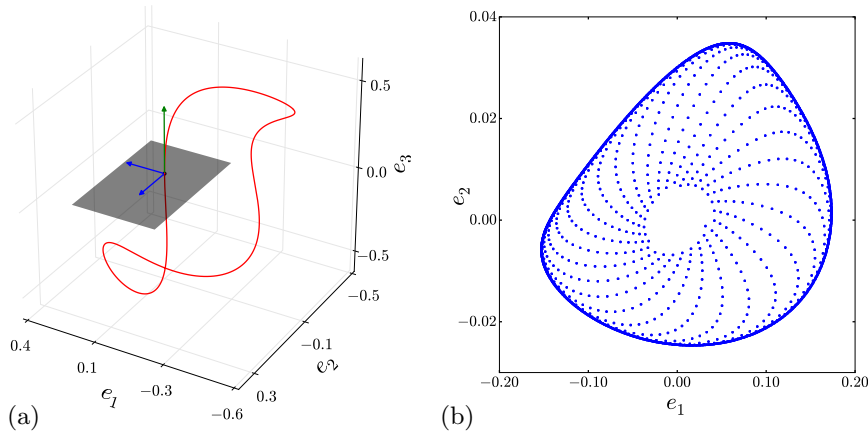
Fig. 3 (a) Pre-periodic orbit p_0 (red), its velocity field $\tilde{v}(\tilde{a}_{p_0})$ at the starting point (green), orthogonal vectors that span the eigenplane corresponding to the leading Floquet vectors (blue) and the Poincaré section hyperplane (gray, transparent). (b) Spiral-out dynamics of a single trajectory in the Poincaré section projected onto (e_1, e_2) plane, system size $L = 21.25$.

In order to study dynamics within the neighborhood of p_0, we define a Poincaré section as the hyperplane of points $\tilde{a}_{\mathcal{P}}$ in an open neighborhood of $\tilde{a}_{p_0}$, orthogonal to the tangent $\tilde{v}(\tilde{a}_{p_0})$ of the orbit at the Poincaré section point,

$$(\tilde{a}_{\mathcal{P}} - \tilde{a}_{p_0}) \cdot \tilde{v}(\tilde{a}_{p_0}) = 0 \quad \text{and} \quad ||\tilde{a}_{\mathcal{P}} - \tilde{a}_{p_0}|| < \alpha \,, \tag{18}$$

where $||.||$ denotes the Euclidean (or $L2$) norm, and the threshold α is empirically set to $\alpha = 0.9$ throughout. The locality condition in (18) is a computationally convenient way to avoid Poincaré section border [18, 19], defined as the set of points $\tilde{a}_{\mathcal{P}}^*$ that satisfy the hyperplane condition $(\tilde{a}_{\mathcal{P}}^* - \tilde{a}_{p_0}) \cdot \tilde{v}(\tilde{a}_{p_0}) = 0$, but their orbits do not intersect this hyperplane transversally, i.e. $\tilde{v}(\tilde{a}_{\mathcal{P}}^*) \cdot \tilde{v}(\tilde{a}_{p_0}) = 0$.

From here on, we study the discrete time dynamics induced by the flow on the Poincaré section (18), as visualized in fig. 3 (a).

In fig. 3 and the rest of the state space projections of this paper, projection bases are constructed as follows: Real and imaginary parts of the Floquet vector $\tilde{V}_1$ define an ellipse $\text{Re}[\tilde{V}_1] \cos\phi + \text{Im}[\tilde{V}_1] \sin\phi$ in the neighborhood of $\tilde{a}_{p_0}$, and we pick as the first two projection-subspace spanning vectors the principal axes of this ellipse. As the third vector we take the velocity field $\tilde{v}(\tilde{a}_{p_0})$, and the projection bases (e_1, e_2, e_3) are found by orthonormalization of these vectors via the Gram-Schmidt procedure. All state space projections are centered on $\tilde{a}_{p_0}$, i.e., $\tilde{a}_{p_0}$ is the origin of all Poincaré section projections.

As an example, we follow a single trajectory starting from $\tilde{a}_{p_0} + 10^{-1}\text{Re}[\tilde{V}_1]$ as it connects to the 2-torus surrounding the periodic orbit in fig. 3 (b). For fig. 3 (b) and all figures to follow, the two leading non-marginal Floquet multipliers of p_0, p_1 and p_2 are listed in table 1. For system size $L = 21.25$ the complex unstable Floquet multiplier pair is nearly marginal, $|\Lambda_{1,2}| = 1.00636$, hence the spiral-out is
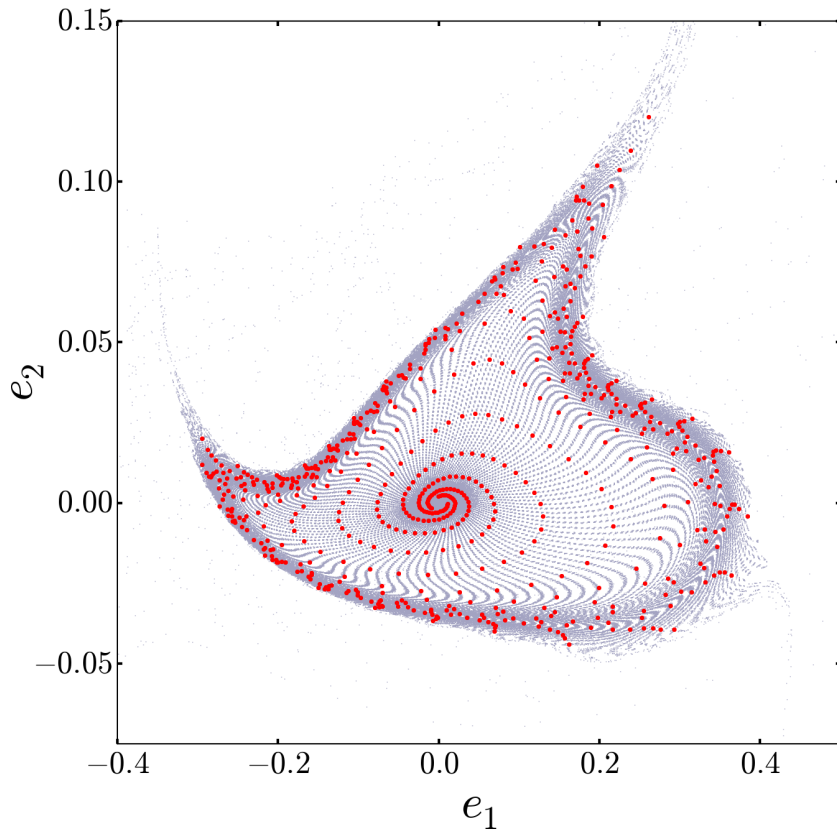
Fig. 4 Unstable manifold (gray) of p_0 on the Poincaré section (18) and an individual trajectory (red) within, system size $L = 21.30$.

very slow. Assume that $\delta\tilde{a}(0)$ is a small perturbation to $\tilde{a}_{p_0}$ that lies in the plane spanned by $(\mathrm{Re}\,[\tilde{V}_1], \mathrm{Im}\,[\tilde{V}_1])$. Then there exists a coefficient vector $c = (c_1, c_2)^T$, with which we can express $\delta\tilde{a}(0)$ in this plane as

$$\delta\tilde{a}(0) = Wc\,, \tag{19}$$

where $W = [\mathrm{Re}\,[\tilde{V}_1], \mathrm{Im}\,[\tilde{V}_1]]$ has real and imaginary parts of the Floquet vector $\tilde{V}_1$ on its columns. Without a loss of generality, we can rewrite c as $c = \delta r R(\theta) c^{(1)}$, where $c^{(1)} = (1, 0)^T$ and $R(\theta)$ is a $[2 \times 2]$ rotation matrix. Thus (19) can be expressed as $\delta\tilde{a}(0) = \delta r W R(\theta) c^{(1)}$. In the linear approximation, discrete time dynamics $\delta\tilde{a}(nT_{p_0})$ is given by

$$\delta\tilde{a}(nT_{p_0}) = |\Lambda_1|^n \delta r W R(\theta - n \arg \Lambda_1) c^{(1)}\,, \tag{20}$$

which can then be projected onto the Poincaré section (18) by acting from the left with the projection operator

$$\mathbb{P}(\tilde{a}_{\mathcal{P}}) = \mathbf{1} - \frac{\tilde{v}(\tilde{a}_{\mathcal{P}}) \otimes \tilde{v}(\tilde{a}_{p_0})}{\langle \tilde{v}(\tilde{a}_{\mathcal{P}}), \tilde{v}(\tilde{a}_{p_0}) \rangle}\,, \tag{21}$$

computed at $\tilde{a}_{\mathcal{P}} = \tilde{a}_{p_0}$. In (21), $\otimes$ denotes the outer product. Defining $\delta\tilde{a}_{\mathcal{P}} \equiv \mathbb{P}(\tilde{a}_{\mathcal{P}})\delta\tilde{a}$ for a small perturbation $\delta\tilde{a}$ to the point $\tilde{a}_{\mathcal{P}}$ on the Poincaré section, discrete time dynamics of $\delta\tilde{a}_{\mathcal{P}}$ in the Poincaré section is given by

$$\delta\tilde{a}_{\mathcal{P}}[n] = |\Lambda_1|^n \delta r W_{\mathcal{P}} R(\theta - n \arg \Lambda_1) c^{(1)} \,, \tag{22}$$

where $W_{\mathcal{P}} = [\mathrm{Re}\,[\tilde{V}_{1,\mathcal{P}}], \mathrm{Im}\,[\tilde{V}_{1,\mathcal{P}}]] = \mathbb{P}(\tilde{a}_{p_0})W$, and n is the discrete time variable counting returns to the Poincaré section. In the Poincaré section, the solutions (22) define ellipses which expand and rotate respectively by factors of $|\Lambda_1|$ and $\arg \Lambda_1$ at each return. In order to resolve the unstable manifold, we start trajectories on an elliptic band parameterized by (δ, ϕ), such that the starting point in the band comes to the end of it on the first return, hence totality of these points cover the unstable manifold in the linear approximation. Such set of perturbations are given by

$$\delta\tilde{a}_{\mathcal{P}}(\delta, \phi) = \epsilon |\Lambda_1|^\delta W_{\mathcal{P}} R(\phi) c^{(1)} \,, \quad \text{where } \delta \in [0, 1) \,, \phi \in [0, 2\pi) \,, \tag{23}$$

and ϵ is a small number. We set $\epsilon = 10^{-3}$ and discretize (23) by taking 12 equidistant points in $[0, 1)$ for δ and 36 equidistant points in $[0, 2\pi)$ for ϕ and integrate each $\tilde{a}_{p_0} + \delta\tilde{a}_{\mathcal{P}}(\delta, \phi)$ forward in time. Fig. 4 shows the unstable manifold of p_0 resolved by this procedure at system size $L = 21.30$, for which the torus surrounding p_0 appears to be unstable as the points approaching to it first slow down and then leave the neighborhood in transverse direction. In order to illustrate this better, we marked an individual trajectory in fig. 4 color red. In fig. 5 we show initial points that go into the calculation, and their first three returns in order to illustrate the principle of the method.

Fig. 5 Initial points (black) on the Poincaré section for unstable manifold computation and their first (red), second (green), and third (blue) returns. Inset: zoomed out view of the initial points and their first three returns.
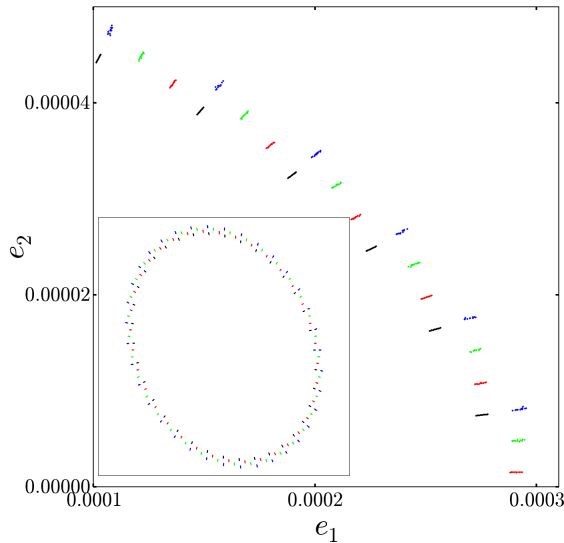
As we continue increasing the system size, we find that at $L \approx 21.36$, trace of the invariant torus disappears and two new periodic orbits p_1 and p_2 emerge in the neighborhood of p_0. Both of these orbits appear as period 3 periodic orbits in the Poincaré map. While p_1 is unstable (found by a Newton search), p_2 is initially

stable with a finite basin of attraction. The unstable manifold of p_0 connects
heteroclinically to the stable manifolds of p_1 and p_2. As we show in fig. 6, resolving
the unstable manifold of p_0 enables us to locate these heteroclinic connections
between periodic orbits. Note that 1-dimensional stable manifold of p_1 separates
the unstable manifold of p_0 in two pieces. Green and blue orbits in fig. 6 appear
to be at two sides of this invariant boundary: while one of them converges to p_2,
the other leaves the neighborhood to explore other parts of the state space that
are not captured by the Poincaré section, following the unstable manifold of p_1.
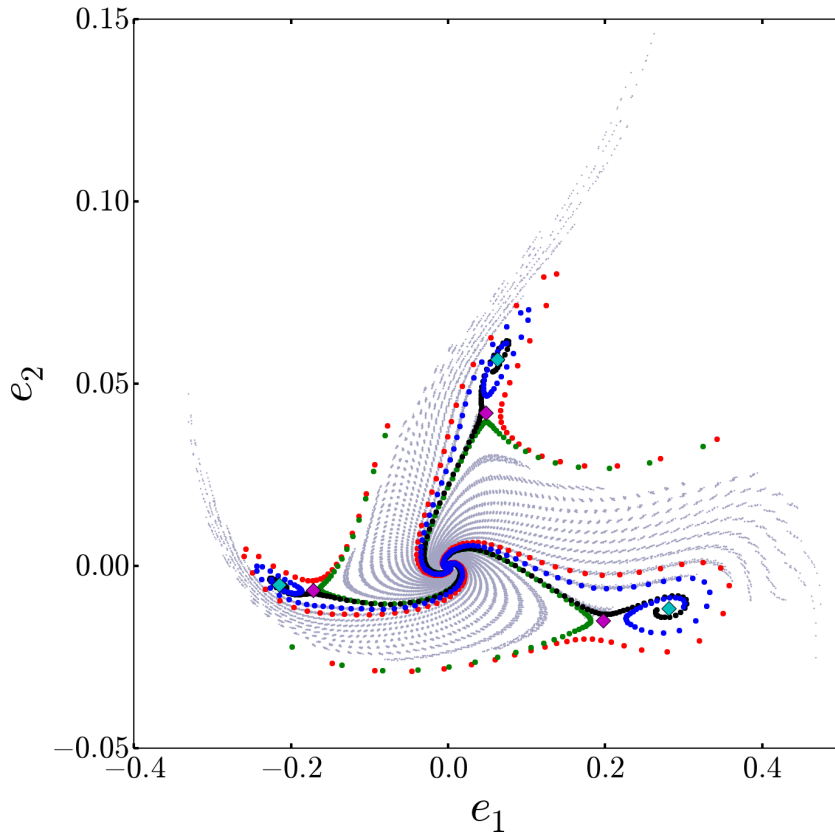
**Fig. 6** Unstable manifold (gray) of p_0 on the Poincaré section (18) at $L = 21.36$. Colored dots
correspond to different individual trajectories within the unstable manifold, with qualitatively
different properties. Diamond shaped markers correspond to the period-3 orbits p_1 (magenta)
and p_2 (cyan).

As the system size is increased, p_2 becomes unstable at $L \approx 21.38$. At $L \approx$
21.477 the two complex unstable Floquet multipliers collide on the real axis and
at $L \approx 21.479$ one of them crosses the unit circle. After this bifurcation, we were no
longer able to continue this orbit. At $L = 21.48$, the spreading of the p_0's unstable
manifold becomes more dramatic, and its boundary is set by the 1-dimensional
unstable manifold of p_1, as shown in fig. 7. We compute the unstable manifold of

p_1 similarly to (23), by integrating

$$\tilde{a}_{\mathcal{P}}(\delta) = \tilde{a}_{p_1,\mathcal{P}} \pm \epsilon \Lambda_1^{\delta} \tilde{V}_{1,\mathcal{P}}, \quad \text{where } \delta \in [0,1). \tag{24}$$

Λ_1 and $\tilde{V}_1$ in (24) are the unstable Floquet multiplier and the corresponding Floquet vector of $\tilde{a}_{p_1}$, and the initial conditions (24) cover the unstable manifold of $\tilde{a}_{p_1}$ in the linear approximation.
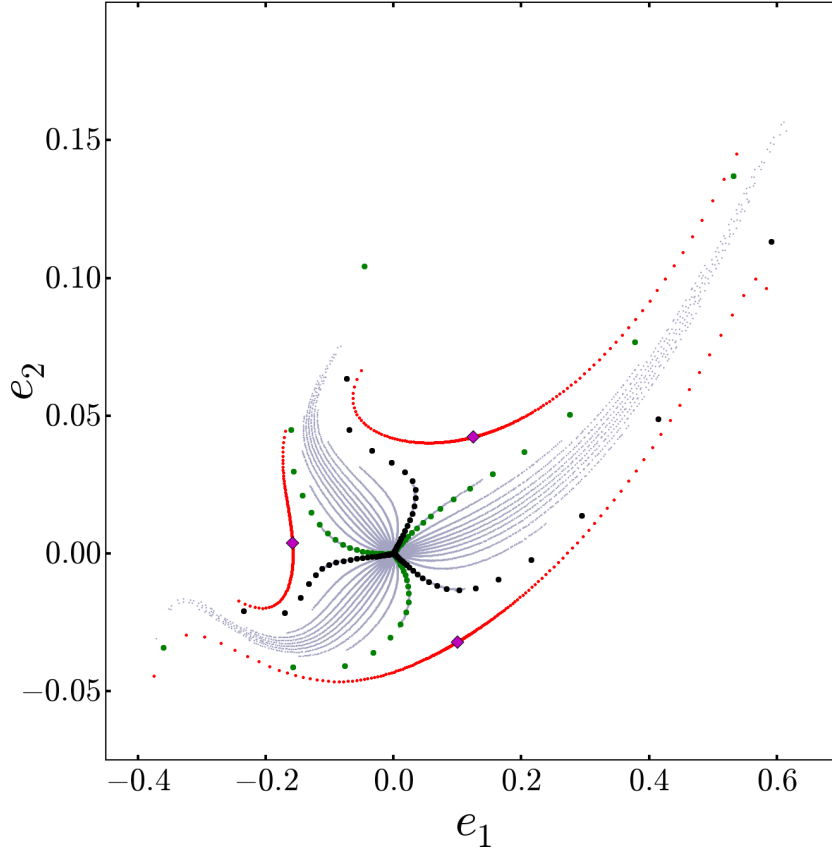
Fig. 7 Unstable manifold of p_0 (gray) and two orbits (black and green) within at $L = 21.48$. Red points lie on the 1-dimensional unstable manifold of p_1 (magenta).

A negative real Floquet multiplier of p_1 crosses the unit circle at $L \approx 21.6$ leading to "drifting" dynamics in the associated unstable direction. Such "symmetry-breaking" bifurcations of relative periodic orbits with C_2 symmetry are ubiquitous in many physical settings: Earlier examples are studies of reduced-order models of convection [38], forced pendulum [20], and Duffing oscillator [48], which reported that symmetry breaking bifurcations precede period doubling route to chaos. A key observation was made by Swift and Wiesenfeld [62], who showed in the context of periodically driven damped pendulum that Poincaré map associated with

the symmetric system is the second iterate of another "reduced" Poincaré map, which identifies symmetry-equivalent points. They then argue that C_2-symmetric periodic orbits generically do not undergo period doubling bifurcations when a single parameter of the system varied. More recent works [6, 44] adapt ref. [62]'s reduced Poincaré map to fluid systems in order to study their bifurcations in the presence of symmetries. For a review of the symmetry-breaking bifurcations in fluid dynamics, see ref. [15].

As in the previous cases, in order to investigate the dynamics of the system at this stage, we compute and visualize the unstable manifold of p_1.

Similarly to (23) and (24), the 2-dimensional unstable manifold of p_1 is approximately covered by initial conditions

$$\tilde{a}_{\mathcal{P}}(\delta, \phi) = \tilde{a}_{p_1, \mathcal{P}} + \epsilon \left[|\Lambda_1|^\delta \cos \phi \, \tilde{V}_{1, \mathcal{P}} + |\Lambda_2|^\delta \sin \phi \, \tilde{V}_{2, \mathcal{P}} \right] \tag{25}$$

where $\delta \in [0, 1)$, $\phi \in [0, 2\pi)$. At system size $L = 21.7$, we set $\epsilon = 10^{-3}$ and discretize (25) by choosing 10 and 36 equally spaced values for δ and ϕ, respectively. First 38 returns of orbits generated according to (25) are shown in fig. 8 as red points along with the unstable manifold of p_0 (gray). Note that, unlike fig. 7, in fig. 8 there is no clear separation on the unstable manifold of p_0. This is because the connection of p_0's unstable manifold to p_1 is no longer captured by the Poincaré section (18) after the unstable manifold of p_1 becomes 2-dimensional. Yet, unstable manifold of p_1 still shapes that of p_0.

Since the leading Floquet exponent μ_1 of p_1 is approximately an order of magnitude larger than μ_2 (see table 1), unstable manifold of p_1 appears as if it is 1-dimensional in fig. 8. However, it is absolutely crucial to study this manifold in 2 dimensions as different initial conditions in this 2-dimensional manifold connect to the regions of state space with qualitatively different dynamics. In order to illustrate this point, we have marked two individual trajectories on the unstable manifold of p_1 with black and green in fig. 8. After observing that these orbits have nearly recurrent dynamics, we ran Newton searches in their vicinity and found two new periodic orbits p_3 and p_4, marked respectively with cyan and yellow diamonds on fig. 8. In the full state space p_3 is a pre-periodic orbit (9), whereas p_4 is a relative periodic orbit (7) with a non-zero drift. We show a time segment of the orbit marked green on fig. 8 without symmetry reduction, as color-coded amplitude of the scalar field $u(x, \tau)$ in fig. 9 (a). For comparison we also show two repeats of p_1 (bottom) and p_4 (top) in fig. 9 (b). Fig. 9 suggests that this orbit leaves the neighborhood of p_1 following a heteroclinic connection to p_4.

In fig. 8, some of the red points appear on the unstable manifold of p_0. These points corresponds to trajectories that leave the unstable manifold of p_1, come back after exploring other parts of the state space and follow unstable manifold of p_0. We could have excluded these points by showing shorter trajectories for higher values of δ in (25) in fig. 8, however we chose not to do so in order to stress that visualizations of unstable manifolds of periodic orbits are not restricted to the dynamics within a small neighborhood of a periodic orbit, but in fact they illuminate the geometry of the flow in a finite part of the strange attractor.

An interesting feature of the bifurcation scenario studied here is the apparent destabilization of the invariant torus before its breakdown. Note that in fig. 4 the trajectories within the unstable manifold of p_0 diverge in normal direction from the region that was inhabited by a stable 2-torus for lower values of L. This suggest
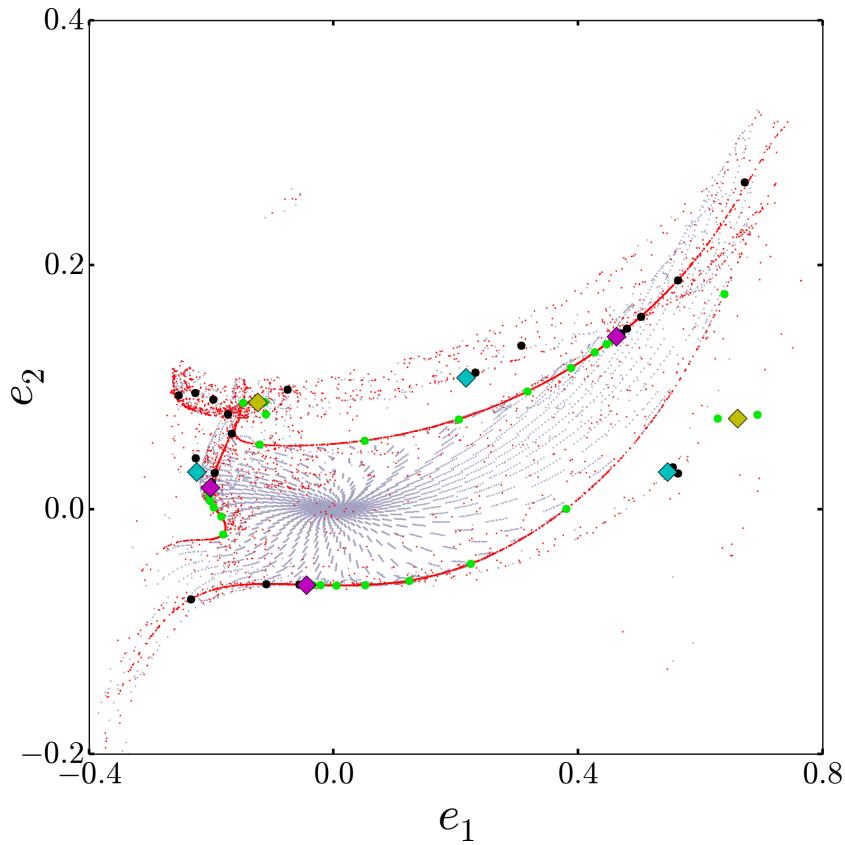
Fig. 8 Unstable manifolds of p_0 (gray) and p_1 (red) on the Poincaré section (18) at $L = 21.7$. Magenta, cyan, and yellow diamond markers respectively indicate the Poincaré section points of p_1, p_3, and p_4. Green and black dots correspond to two individual orbits started on the linear approximation to the unstable manifold of p_1, which visit neighborhoods of p_3 and p_4 respectively.

that the invariant torus has become normally hyperbolic [23]. This torus could be computed by the method of ref. [42], but our goal here is more modest, what we have computed already amply demonstrates the utility of our O(2) symmetry reduction. Note also that the stable period-3 orbit p_2 in fig. 6 has a finite basin of attraction, and the trajectories which do not fall into it leave its neighborhood. In typical scenarios involving generation of stable - unstable pairs of periodic orbits within an invariant torus (see e.g. ref. [2]), the torus becomes a heteroclinic connection between the periodic orbit pair. Here the birth of the period-3 orbits appears to destroy the torus.

5 Summary and future directions

The two main results presented here are: 1) a new method for reducing the O(2)-symmetry of PDEs, and 2) a symmetry-reduced state space Poincaré   section
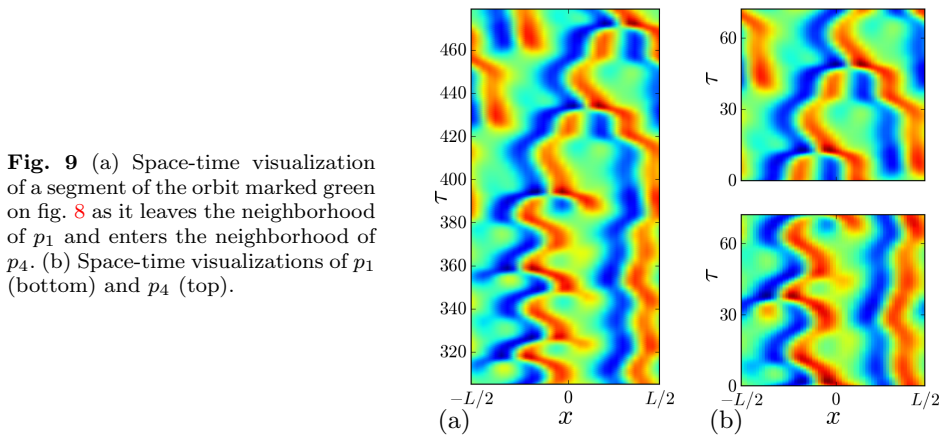
Fig. 9 (a) Space-time visualization of a segment of the orbit marked green on fig. 8 as it leaves the neighborhood of p_1 and enters the neighborhood of p_4. (b) Space-time visualizations of p_1 (bottom) and p_4 (top).

visualization of 1- and 2-dimensional unstable manifolds of Kuramoto-Sivashinsky periodic orbits.

Our method for the computation of unstable manifolds is general and can find applications in many other ODE and PDE settings. The main idea here is a generalization of Gibson *et al.* [27] method for visualizations of the unstable manifolds of equilibria, originally applied to plane Couette flow, a setting much more complex then the current paper. All our computations are carried out for the full Kuramoto-Sivashinsky equation (1), in 30 dimensions, and it is remarkable how much information is captured by the 2- and 3-dimensional projections of the O(2) symmetry-reduced Poincaré sections - none of that structure is visible in the full state space.

The Kuramoto-Sivashinsky O(2) symmetry reduction method described here might require modifications when applied to other problems. For example, for PDEs of space dimensions larger then one, there can be more freedom in choosing the phase fixing condition (10). This indeed is the case for shear flows with both homogeneous (streamwise and spanwise translation invariant) and inhomogeneous (wall-normal) directions. When adapting the first Fourier mode slice method to such problems, one should experiment with the dependence of the phase fixing condition on the inhomogeneous coordinate such that the slice fixing phase is uniquely defined for state space regions of interest; see chapter 3 of ref. [8] for details. Ref. [67] makes this choice for pipe flow by taking a 'typical state' in the turbulent flow, setting all streamwise Fourier modes other than the first one to zero, and using this state as a "slice template". Another point to be taken into consideration for canonical shear flows is that their symmetry group is SO(2) × O(2). So far, continuous symmetry reduction in pipe flows [66, 67] were confined to settings, where an imposed symmetry in conjugacy class of spanwise reflection disallows spanwise rotations. When no such restriction is present, one needs two conditions for fixing both streamwise and spanwise translations. These conditions must be chosen such that the order at which continuous symmetries are reduced does not matter. For direct products of commuting SO(2) symmetries, this is a straightforward task and outlined in section 3 of ref. [8]. An application of these ideas to the pipe flow is going to appear in a future publication [9].

Furthermore, while invariant polynomials similar to (16) can be constructed for any problem with a reflection symmetry, an intermediate step is necessary if the action of reflection σ symmetry is not the sign flip of a subset of coordinates. In that case, one should first decompose the state space into symmetric and antisymmetric subspaces by computing $a_S = (1/2)[a + D(\sigma)a]$ and $a_A = (1/2)[a - D(\sigma)a]$, respectively, and construct invariants analogous to (16) for elements of a_A that are not strictly zero. Generalizations of this approach to richer discrete symmetries, such as dihedral groups, remains an open problem, with potential application to systems such as the Kolmogorov flow [22, 49].

Bifurcation scenarios similar to the one studied here are ubiquitous in high-dimensional systems. For example, Avila *et al.* [5] study of transition to turbulence in pipe flow, and Zammert and Eckhardt's study of the plane Poiseuille flow [68] both report torus bifurcations of relative periodic orbits along transitions to chaos. We believe that the methods presented in this paper can lead to a deeper understanding of these scenarios.

While unstable manifold visualizations of periodic orbits in the symmetry-reduced state space illustrates bifurcations of these orbits, our motivation for investigating such objects is not a study of bifurcations, but ultimately a partition of the turbulent flow's state space into qualitatively different regions, and construction of the corresponding symbolic dynamics. Fig. 8 and fig. 9 demonstrate our progress in this direction: we are able to identify symmetry breaking heteroclinic connections from non-drifting solutions to the drifting ones. Such observations would have been very hard to make without reducing symmetries of the system, since each relative periodic orbit has a reflection copy, corresponding to a solution drifting in the other direction; and each such solution has infinitely many copies obtained by translations.

A Computational details

Throughout this paper, we used the 16 Fourier mode truncation of Kuramoto-Sivashinsky equation (2), which renders the state space 30-dimensional. Sufficiency of this truncation was demonstrated for $L = 22$ in ref. [17]. In all our computations, we integrate (12) and its gradient system numerically, using a general purpose adaptive integrator `odeint` from `scipy.integrate` [35], which is a wrapper of `lsoda` from `ODEPACK` library [32]. Note that (12) is singular if $\hat{b}_1 = 0$, i.e., whenever the first Fourier mode vanishes. This singularity can be regularized by a time-rescaling if a fixed time step integrator is desired [11].

Transformation of trajectories and tangent vectors to the fully symmetry-reduced state space (17) is applied as post-processing. For a trajectory $\hat{a}(\tau)$, we simply apply the reflection reducing transformation to obtain the trajectory as $\tilde{a}(\tau) = \tilde{a}(\hat{a}(\tau))$. Velocity field (12) transforms to (17) by acting with the Jacobian matrix

$$\tilde{v}(\tilde{a}) = \frac{d\tilde{a}(\hat{a})}{d\hat{a}} \hat{v}(\hat{a}) \,.$$

Floquet vectors transform to the fully symmetry-reduced state space similarly, however, their computations in the first Fourier mode slice requires some care. Remember that the reflection symmetry remains after the continuous symmetry reduction, and its action is represented by (13). Thus, denoting finite time flow induced by (12) by $\hat{f}^\tau(\hat{a})$, pre-periodic orbit within the slice satisfies

$$\hat{a}_{pp} = \hat{D}(\sigma)\hat{f}^{T_p}(\hat{a}_{pp}) \,,$$

with its linear stability given by the spectrum of the Jacobian matrix

$$\hat{J}_{pp} = \hat{D}(\sigma)\hat{J}^{T_p}(\hat{a}_{pp}),$$

where $\hat{J}^{T_p}(\hat{a}_{pp})$ is the Jacobian matrix of the flow function $\hat{f}^{T_p}(\hat{a}_{pp})$. Thus, in order to find the Floquet vectors in fully symmetry-reduced representation, we first find the eigenvectors $\hat{V}$ of the Jacobian matrix $\hat{J}_{pp}$ and then transform them as $\tilde{V}(\tilde{a}) = d\tilde{a}(\hat{a}_{pp})/d\hat{a}\,\hat{V}(\hat{a})$.

References

[1] D. Armbruster, J. Guckenheimer, and P. Holmes, "Kuramoto-Sivashinsky dynamics on the center-unstable manifold", SIAM J. Appl. Math. **49**, 676–691 (1989).

[2] V. I. Arnold, *Geometrical Methods in the Theory of Ordinary Differential Equations* (Springer, Berlin, 1982).

[3] R. Artuso, E. Aurell, and P. Cvitanović, "Recycling of strange sets: I. Cycle expansions", Nonlinearity **3**, 325–359 (1990).

[4] R. Artuso, E. Aurell, and P. Cvitanović, "Recycling of strange sets: II. Applications", Nonlinearity **3**, 361–386 (1990).

[5] M. Avila, F. Mellibovsky, N. Roland, and B. Hof, "Streamwise-localized solutions at the onset of turbulence in pipe flow", Phys. Rev. Lett. **110**, 224502 (2013).

[6] H. M. Blackburn, F. Marques, and J. M. Lopez, "Symmetry breaking of two-dimensional time-periodic wakes", J. Fluid Mech. **522**, 395–411 (2005).

[7] R. Bowen, *Equilibrium States and the Ergodic Theory of Anosov Diffeomorphisms* (Springer, Berlin, 1975).

[8] N. B. Budanur, Exact Coherent Structures in Spatiotemporal Chaos: From Qualitative Description to Quantitative Predictions, PhD thesis (School of Physics, Georgia Inst. of Technology, Atlanta, 2015).

[9] N. B. Budanur and B. Hof, State space geometry of the laminar-turbulent boundary in pipe flow, in preparation, 2017.

[10] N. B. Budanur, D. Borrero-Echeverry, and P. Cvitanović, "Periodic orbit analysis of a system with continuous symmetry - A tutorial", Chaos **25**, 073112 (2015).

[11] N. B. Budanur, P. Cvitanović, R. L. Davidchack, and E. Siminos, "Reduction of the SO(2) symmetry for spatially extended dynamical systems", Phys. Rev. Lett. **114**, 084102 (2015).

[12] E. Cartan, *La méthode du repère mobile, la théorie des groupes continus, et les espaces généralisés*, Vol. 5, Exposés de Géométrie (Hermann, Paris, 1935).

[13] P. Chossat and R. Lauterbach, *Methods in Equivariant Bifurcations and Dynamical Systems* (World Scientific, Singapore, 2000).

[14] F. Christiansen, P. Cvitanović, and V. Putkaradze, "Spatiotemporal chaos in terms of unstable recurrent patterns", Nonlinearity **10**, 55–70 (1997).

[15] J. D. Crawford and E. Knobloch, "Symmetry and symmetry-breaking bifurcations in fluid dynamics", Ann. Rev. Fluid Mech. **23**, 341–387 (1991).

[16] P. Cvitanović, "Invariant measurement of strange sets in terms of cycles", Phys. Rev. Lett. **61**, 2729–2732 (1988).

[17] P. Cvitanović, R. L. Davidchack, and E. Siminos, "On the state space geometry of the Kuramoto-Sivashinsky flow in a periodic domain", SIAM J. Appl. Dyn. Syst. **9**, 1–33 (2010).

[18] P. Cvitanović, D. Borrero-Echeverry, K. Carroll, B. Robbins, and E. Siminos, "Cartography of high-dimensional flows: A visual guide to sections and slices", Chaos **22**, 047506 (2012).

[19] P. Cvitanović, R. Artuso, R. Mainieri, G. Tanner, and G. Vattay, *Chaos: Classical and Quantum* (Niels Bohr Inst., Copenhagen, 2016).

[20] D. D'Humieres, M. R. Beasley, B. A. Huberman, and A. Libchaber, "Chaotic states and routes to chaos in the forced pendulum", Phys. Rev. A **26**, 3483–3496 (1982).

[21] Y. Duguet, A. P. Willis, and R. R. Kerswell, "Transition in pipe flow: the saddle structure on the boundary of turbulence", J. Fluid Mech. **613**, 255–274 (2008).

[22] M. Farazmand, "An adjoint-based approach for finding invariant solutions of Navier-Stokes equations", J. Fluid M. **795**, 278–312 (2016).

[23] N. Fenichel, "Persistence and smoothness of invariant manifolds for flows", Indiana Univ. Math. J. **21**, 193–226 (1971).

[24] M. J. Field, "Equivariant dynamical systems", Trans. Amer. Math. Soc. **259**, 185–205 (1980).

[25] K. Gatermann, *Computer Algebra Methods for Equivariant Dynamical Systems* (Springer, New York, 2000).

[26] J. F. Gibson, Channelflow: A spectral Navier-Stokes simulator in C++, tech. rep., `Channelflow.org` (U. New Hampshire, 2013).

[27] J. F. Gibson, J. Halcrow, and P. Cvitanović, "Visualizing the geometry of state-space in plane Couette flow", J. Fluid Mech. **611**, 107–130 (2008).

[28] R. Gilmore and C. Letellier, *The Symmetry of Chaos* (Oxford Univ. Press, Oxford, 2007).

[29] J. M. Greene and J.-S. Kim, "The steady states of the Kuramoto-Sivashinsky equation", Physica D **33**, 99–120 (1988).

[30] M. C. Gutzwiller, "Periodic orbits and classical quantization conditions", J. Math. Phys. **12**, 343–358 (1971).

[31] D. Hilbert, "Über die vollen Invariantensysteme", Math. Ann. **42**, 313–373 (1893).

[32] A. C. Hindmarsh, "ODEPACK, a systematized collection of ODE solvers", in *Scientific Computing*, Vol. 1, edited by R. S. Stepleman (North-Holland, Amsterdam, 1983), pp. 55–64.

[33] P. Holmes, J. L. Lumley, and G. Berkooz, *Turbulence, Coherent Structures, Dynamical Systems and Symmetry* (Cambridge Univ. Press, Cambridge, 1996).

[34] E. Hopf, "Abzweigung einer periodischen Lösung", Bereich. Sächs. Acad. Wiss. Leipzig, Math. Phys. Kl. **94**, 19 (1942).

[35] E. Jones, T. Oliphant, P. Peterson, et al., SciPy: Open source scientific tools for Python, 2001.

[36] L. Kadanoff and C. Tang, "Escape rate from strange repellers", Proc. Natl. Acad. Sci. USA **81**, 1276–1279 (1984).

[37] I. G. Kevrekidis, B. Nicolaenko, and J. C. Scovel, "Back in the saddle again: a computer assisted study of the Kuramoto-Sivashinsky equation", SIAM J. Appl. Math. **50**, 760–790 (1990).

[38] E. Knobloch and N. Weiss, "Bifurcations in a model of double-diffusive convection", Phys. Let. A **85**, 127–130 (1981).

[39] M. Krupa, "Bifurcations of relative equilibria", SIAM J. Math. Anal. **21**, 1453–1486 (1990).

[40] Y. Kuramoto and T. Tsuzuki, "Persistent propagation of concentration waves in dissipative media far from thermal equilibrium", Progr. Theor. Phys. **55**, 356–369 (1976).

[41] Y. Lan and P. Cvitanović, "Unstable recurrent patterns in Kuramoto-Sivashinsky dynamics", Phys. Rev. E **78**, 026208 (2008).

[42] Y. Lan, C. Chandre, and P. Cvitanović, "Variational method for locating invariant tori", Phys. Rev. E **74**, 046206 (2006).

[43] R. Mainieri and P. Cvitanović, "A brief history of chaos", in *Chaos: Classical and Quantum* (Niels Bohr Inst., Copenhagen, 2016).

[44] F. Marques, J. M. Lopez, and H. M. Blackburn, "Bifurcations in systems with Z2 spatio-temporal and O(2) spatial symmetry", Physica D **189**, 247–276 (2004).

[45] R. Miranda and E. Stone, "The proto-Lorenz system", Phys. Lett. A **178**, 105–113 (1993).

[46] J. Neimark, "On some cases of periodic motions depending on parameters", Dokl. Akad. Nauk SSSR **129**, in Russian, 736–739 (1959).

[47] E. Noether, "Der Endlichkeitssatz der Invarianten endlicher Gruppen", Math. Ann. **77**, 89–92 (1915).

[48] S. Novak and R. G. Frehlich, "Transition to chaos in the Duffing oscillator", Phys. Rev. A **26**, 3660–3663 (1982).

[49] N. Platt, L. Sirovich, and N. Fitzmaurice, "An investigation of chaotic Kolmogorov flows", Phys. Fluids A **3**, 681–696 (1991).

[50] E. L. Rempel and A. C. Chian, "Intermittency induced by attractor-merging crisis in the Kuramoto-Sivashinsky equation", Phys. Rev. E **71**, 016203 (2005).

[51] E. L. Rempel, A. C. Chian, E. E. Macau, and R. R. Rosa, "Analysis of chaotic saddles in high-dimensional dynamical systems: the Kuramoto-Sivashinsky equation", Chaos **14**, 545–56 (2004).

[52] E. L. Rempel, A. C. Chian, and R. A. Miranda, "Chaotic saddles at the onset of intermittent spatiotemporal chaos", Phys. Rev. E **76**, 056217 (2007).

[53] D. Ruelle, "Generalized zeta-functions for Axiom A basic sets", Bull. Amer. Math. Soc **82**, 153–156 (1976).

[54] D. Ruelle, "Zeta-functions for expanding maps and Anosov flows", Inv. Math. **34**, 231–242 (1976).

[55] R. J. Sacker, "A new approach to the perturbation theory of invariant surfaces", Commun. Pure Appl. Math. **18**, 717–732 (1965).

[56] T. M. Schneider, B. Eckhardt, and J. Yorke, "Turbulence, transition, and the edge of chaos in pipe flow", Phys. Rev. Lett. **99**, 034502 (2007).

[57] E. Siminos, Recurrent spatio-temporal structures in presence of continuous symmetries, PhD thesis (School of Physics, Georgia Inst. of Technology, Atlanta, 2009).

[58] E. Siminos and P. Cvitanović, "Continuous symmetry reduction and return maps for high-dimensional flows", Physica D **240**, 187–198 (2011).

[59] G. I. Sivashinsky, "Nonlinear analysis of hydrodynamical instability in laminar flames - I. Derivation of basic equations", Acta Astronaut. **4**, 1177–1206 (1977).

[60] J. D. Skufca, J. A. Yorke, and B. Eckhardt, "Edge of Chaos in a parallel shear flow", Phys. Rev. Lett. **96**, 174101 (2006).

[61] S. Smale, "Differentiable dynamical systems", Bull. Amer. Math. Soc. **73**, 747–817 (1967).

[62] J. W. Swift and K. Wiesenfeld, "Suppression of period doubling in symmetric systems", Phys. Rev. Lett. **52**, 705–708 (1984).

[63] S. Toh and T. Itano, "A periodic-like solution in channel flow", J. Fluid Mech. **481**, 67–76 (2003).

[64] R. F. Williams, "The structure of Lorenz attractors", Publ. Math. IHES **50**, 73–99 (1979).

[65] A. P. Willis, Openpipeflow: Pipe flow code for incompressible flow, tech. rep., `Openpipeflow.org` (U. Sheffield, 2014).

[66] A. P. Willis, P. Cvitanović, and M. Avila, "Revealing the state space of turbulent pipe flow by symmetry reduction", J. Fluid Mech. **721**, 514–540 (2013).

[67] A. P. Willis, K. Y. Short, and P. Cvitanović, "Symmetry reduction in high dimensions, illustrated in a turbulent pipe", Phys. Rev. E **93**, 022204 (2016).

[68] S. Zammert and B. Eckhardt, "Crisis bifurcations in plane Poiseuille flow", Phys. Rev. E **91**, 041003 (2015).